



**HAL**  
open science

## Surfaces based on amino acid functionalized polyelectrolyte films towards active surfaces for enzyme immobilization

Ximena Briones, Valeria Villalobos, Yves Queneau, Caroline Silva Danna, Rodrigo Muñoz, Hernán Ríos, Jorge Pavez, Maritza Páez, Ricardo Cabrera, Laura Tamayo, et al.

### ► To cite this version:

Ximena Briones, Valeria Villalobos, Yves Queneau, Caroline Silva Danna, Rodrigo Muñoz, et al.. Surfaces based on amino acid functionalized polyelectrolyte films towards active surfaces for enzyme immobilization. *Materials Science and Engineering: C*, 2019, 104, pp.109938. 10.1016/j.msec.2019.109938 . hal-02193218

**HAL Id: hal-02193218**

**<https://udl.hal.science/hal-02193218>**

Submitted on 8 Jul 2020

**HAL** is a multi-disciplinary open access archive for the deposit and dissemination of scientific research documents, whether they are published or not. The documents may come from teaching and research institutions in France or abroad, or from public or private research centers.

L'archive ouverte pluridisciplinaire **HAL**, est destinée au dépôt et à la diffusion de documents scientifiques de niveau recherche, publiés ou non, émanant des établissements d'enseignement et de recherche français ou étrangers, des laboratoires publics ou privés.

# Amino Acid Functionalized Polyelectrolyte Films as Bioactive Surfaces for Cell Adhesion

*M.S. Leal, † X. Briones, † V. Villalobos, † Y. Queneau, ‡ A. Leiva, § H.E. Ríos, † J. Pavez, | C.P. Silva, | C. Carrasco, || Andrónico Neira-Carrillo, ∞ A. Roth, || L. Tamayo, \*† M.D. Urzúa\*†*

† Depto. de Química, Facultad de Ciencias, Universidad de Chile, Las Palmeras 3425, Santiago, Chile

◇ Universidad Autónoma de Chile, Instituto de Ciencias Químicas Aplicadas, Facultad de Ingeniería, El Llano Subercaseaux 2801, San Miguel, Chile

‡ Université de Lyon, ICBMS, UMR 5246, CNRS, UCBL, INSA Lyon, CPE Lyon, Bât. Lederer, 1 Rue Victor Grignard, 69622 Villeurbanne Cedex, France

§ Depto. Química Física, Facultad de Química, Pontificia Universidad Católica de Chile, Macul, Santiago 7820436, Chile

| Depto. de Química de los Materiales, Fac. de Química-Biología, Universidad de Santiago de Chile, Av. B. O'Higgins 3363, Santiago, Chile

|| Departamento de Biología, Facultad de Ciencias, Universidad de Chile, P. C. 780-0023, Santiago, Chile

∞ Fac. de Ciencias Veterinarias y Pecuarias, Universidad de Chile, Av. Sta. Rosa 11735, Santiago, Chile

KEYWORDS: Polyelectrolytes, amino acid, functionalization, cell adhesion, SH-SY5Y

neuroblastoma.

## ABSTRACT

Surfaces were prepared with polyelectrolyte derivatives of poly(styrene-*alt*-maleic anhydride) (PSMA) functionalized with amino acids of different hydropathy indices, with the aim of evaluating the effect of the chemical functionality of polyelectrolytes on SH-SY5Y neuroblastoma cell adhesion. Functionalizing PSMA derivatives with L-glutamine, L-methionine and L-tyrosine yielded PSMA-Gln, PSMA-Met and PSMA-Tyr polyelectrolytes, respectively. We first studied the adsorption behavior of PSMA functionalized with amino acids on silicon wafer surfaces modified with 3-aminopropyltriethoxysilane (APTES) at pH 4.0 and 7.0 and at low and high ionic strength. The highest rate of polyelectrolyte adsorption was at pH 4.0 and high ionic strength, and was higher with the glutamine and tyrosine films. The advance contact angles ( $\theta_A$ ) of the polyelectrolyte surfaces showed a moderate effect of ionic strength and pH on polyelectrolyte film wettability, with PSMA-Tyr being slightly more hydrophobic. AFM images of the polyelectrolyte surfaces showed two types of morphology: the well-defined globular nanostructure of PSMA-Met and PSMA-Tyr, and the densely packed nanofibrous-like structure of PSMA-Gln. The highest level of ionic strength caused a slight decrease in size of the nanostructure that formed the surface domains, which was reflected in the degree of surface roughness. Cell adhesion assays with polyelectrolyte film showed that SH-SY5Y neuroblastoma cells cultured on PSMA-Met present a well-extended morphology characterized by a stellate shape, with five or more actin-rich thin processes, while SH-SY5Y cells that were seeded on PSMA-Gln and PSMA-Tyr have a round morphology, with fewer and shorter processes. These results indicate that it is possible to modulate the surface characteristics of polyelectrolyte films based on their chemical functionality and environmental parameters such as pH and ionic strength, in order to evaluate their effect on cell adhesion. Thus, surfaces prepared from

polyelectrolytes functionalized with amino acids are an attractive and simple platform for cell adhesion, which can be used in developing biomaterials with modulated surface properties.

## 1. INTRODUCTION

Important advances have been made in designing biomaterials for medical implants, supports for cell regeneration and biosensors for disease diagnosis, but there are still challenges to be overcome. Of particular interest are the processes and interactions that occur in the biomaterial-biological system interface, in order to achieve a favorable response of the latter (eukaryotic cell, bacterium, bone or blood). In the search for biological selectivity, it is key to understand biomaterial surface properties and how to modulate them and the responses they elicit from different cell types. Among the most important surface variables are wettability, topography, energy and surface charge.<sup>1</sup> It has been observed that positive surface charge and hydrophilicity enhance 3T3 fibroblast adhesion.<sup>2</sup> Other surface variables like roughness also play an important role, and in general some characteristics has been observed that favors the adhesion of each cell type. In the case of neuronal cell grown on silicon, surface roughness at a nanoscale of 50 to 70 nm favors adhesion.<sup>3</sup>

Given the need to modulate the chemical properties of biomaterial surfaces, polyelectrolytes offer important advantages due to the variety of their chemical functionality and ionizable groups, which allows for controlling their specificity, mainly by electrostatic, dipole-dipole, hydrophobic and hydrogen bonding interactions.<sup>4</sup> The biological selectivity of surfaces is an important characteristic in biological applications, which can be enhanced by modifying polyelectrolytes with biomolecules like carbohydrates, amino sugars, peptides, and others.<sup>5-7</sup>

Arginine-rich peptides have been shown to promote cellular internalization, which has led to multiple modifications of chitosan with arginine to imitate the cellular function of arginine

peptides.<sup>8,9</sup> It has been reported that modification of chitosan grafting with hydrophobic amino acids improves blood compatibility and increases cell viability. These effects are proportional to the increase in the hydrophobicity of chitosan modified with amino acids of different hydropathy indices.

Studies have evaluated the osteogenic capacity of films of chitosan modified with anionic carbohydrates, and have found that the presence of 4-chondroitin sulfate (chondroitin 4-sulfate) promotes BMSC cell proliferation.<sup>10</sup> The modification of chitosan with integrin-binding consensus peptides common to cell matrix proteins like RGD (Arg-Gly-Asp) and GRGD (Gly-Arg-Gly-Asp) increases the adhesion of multiple cell types (e.g. osteosarcoma, osteoblasts and fibroblasts).<sup>11-13</sup> However, functionalization methods for cell adhesion peptides are expensive and often require multiple stages of conjugation. While several studies have demonstrated the advantages of modifying chitosan to promote cell interaction selectivity, chitosan has the disadvantages of low water solubility, *in vivo* de-polymerization and hemo-incompatibility.<sup>14</sup> The ideal polyelectrolyte would be stable over a wide pH range, and would require simple and inexpensive modification methods.

Polyelectrolytes like maleic anhydride derivatives have the advantage of a high degree of water solubility over a wide pH range, in addition to being biologically active.<sup>15</sup> The high degree of reactivity of the co-monomer maleic anhydride allows the synthesis of alternating copolymers that can be used as platforms for functional modulation, providing a high degree of chemical versatility that can be enhanced by modification with biomolecules that favor the required biological response.<sup>16</sup> Given the reactivity of the maleic anhydride co-monomer and the easiness of synthesizing alternating copolymers, in addition to their water solubility and excellent biocompatibility, the use of these copolymers as platforms for the covalent attachment of amino

acids, allows to obtain functionalized polyelectrolytes with enhanced properties such as, their biocompatibility and therefore would allow for the development of active surfaces that promote cell adhesion.

Polymeric films were developed in this work based on poly(maleic anhydride-*alt*-styrene) [PSMA] modified with amino acids of different hydrophobic indices (H): L-glutamine (H = -3.5), L-tyrosine (H = -1.3) and L-methionine (H = 1.9),<sup>17</sup> with the aim of evaluating the effect of modifying film surface properties (wettability, surface energy, hysteresis, roughness and charge density) on the adhesion of human SH-SY5Y neuroblastoma cells. The human neuroblastoma SH-SY5Y has served as a robust in vitro model of multiple neuronal events such as migration, differentiation and neuritogenesis.<sup>18,19</sup> They are sensible to different stimuli which has made it particularly well suited for study the neuron-to-substrates interactions.<sup>20</sup> Thus, taking advantage of the sensibility of SH-SY5Y cells we evaluated their response the physicochemical characteristics of modified PSMA-substrates.

## **EXPERIMENTAL SECTION**

### **2.1 Materials**

The monomers maleic anhydride (MA) and styrene (S); the amino acids L-glutamine (reagent grade >99% TLC), L-methionine (>98% TLC) and L-tyrosine (reagent grade >98%, TLC); and 3-aminopropyltriethoxysilane (APTES, > 98%) were obtained commercially from Sigma-Aldrich. The NaCl and NaHCO<sub>3</sub> salts and all the solvents used, including benzene, dimethylsulfoxide (DMSO), ethanol, 25% ammonium hydroxide, hydrogen peroxide and deuterated dimethylsulfoxide (DMSO-D<sub>6</sub>) were obtained commercially from Merck. Silicon wafers were obtained commercially from Silicon Quest, USA.

Deionized water of 0.055  $\mu\text{S}/\text{cm}$  conductivity, 18.2  $\text{M}\Omega\text{cm}$  resistivity and TOC (total organic carbon) content below 10 ppb obtained from a LabStar 4-DI deionizer was used to prepare the aqueous solutions.

## **2.2 Poly(maleic anhydride-*alt*-styrene) Synthesis**

Poly(maleic anhydride-*alt*-styrene) copolymer, PSMA, with a molecular weight of  $M_v=6.3 \times 10^4$  g/mol, was synthesized by radical polymerization by mixing equimolar amounts of previously purified styrene and maleic anhydride monomers, obtaining an alternate copolymer given by the value of the reactivity ratio of the co-monomers which is approximately equal to zero.<sup>21</sup> Anhydrous benzene was used as a solvent, and 8% of  $\alpha,\alpha$ -azobisisobutyronitrile (AIBN) was used as the initiator. The synthesis was carried out at 60 °C in an  $\text{N}_2$  atmosphere for 2 h.

## **2.3 Determining Molecular Weight**

The average viscosimetric molecular weight ( $M_v$ ) of the PSMA polymer of 63.000 g/mol was determined by measuring the viscosity of PSMA solutions with THF as a solvent at 30 °C. The weight was calculated with the Mark-Houwink-Sakurada equation, using the constants  $a=0.81$  and  $k=5.07 \times 10^{-5}$ .<sup>22,23</sup> A polydispersity value of 1.7 was obtained. Polydispersity was obtained using size exclusion chromatography (SEC) using a Waters Styragel HMW-6E column, solutions of 1 mg/mL in tetrahydrofuran as solvent and polystyrene standards (18200, 42300, 83000 and 189000 Da) with a flow of 0.3 mL/min.

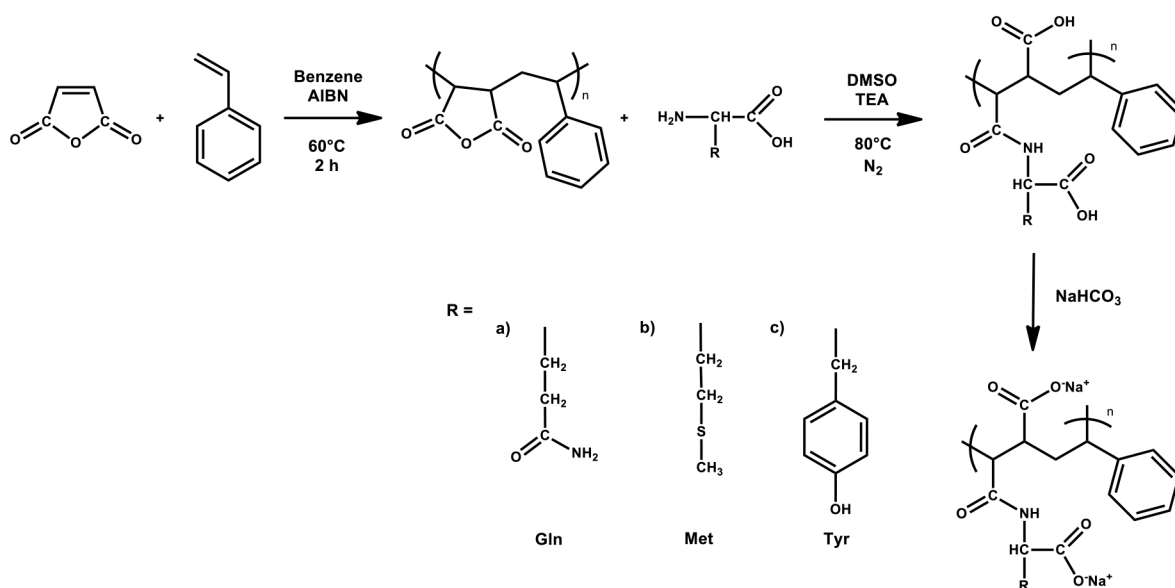
## **2.4 Functionalizing PSMA with Amino Acids**

The PSMA copolymer was functionalized by mixing equimolar amounts of PSMA with the amino acids L-glutamine (Gln), L-methionine (Met) and L-tyrosine (Tyr), using DMSO as the solvent and 0.3 % triethylamine (TEA) as a base at a constant temperature of 80 °C, under an  $\text{N}_2$  atmosphere (Scheme 1). The progress of the modification reactions was monitored by FT-IR

spectroscopy. The final stage of the reaction was established when the bands at  $1854\text{ cm}^{-1}$  and  $1779\text{ cm}^{-1}$ , which belong to the two carbonyl groups of maleic anhydride, disappeared and bands that belong to the carbonyls of the amide and carboxylic acid groups were observed at  $\sim 1660\text{ cm}^{-1}$  and  $\sim 1710\text{ cm}^{-1}$ , respectively.<sup>24</sup>

The disodium salts of the modified polymers were obtained by treating them with aqueous solutions of  $\text{NaHCO}_3$  (in a 1:2 polymer: $\text{NaHCO}_3$  ratio) for 10 days. The solutions were then ultrafiltered and lyophilized. The salts of the polyelectrolytes obtained with the amino acids, L-glutamine, L-methionine and L-tyrosine, were respectively labeled PSMA-Gln, PSMA-Met and PSMA-Tyr. Their structures are represented in Scheme 2.

**Scheme 1.** Reactions to obtain salts from polyelectrolytes derived from PSMA modified with amino acids. R represents the side groups of the amino acids: a) glutamine, b) methionine and c) tyrosine.



## **2.5 FT-IR Spectroscopy**

KBr discs were prepared with 2 mg of polymer and 100 mg of KBr to characterize pure PSMA and copolymers functionalized with amino acids. The FT-IR spectra were obtained with a Bruker Vector Model 22 at 25°C. The spectra were collected at 4 cm<sup>-1</sup> data intervals (scanner velocity: 10 kHz; background: 32 scans; sample: 32 scans). The calibration model for PSMA and functionalized PSMA was built with Bruker OPUS version 6.5 software (Bruker, Ettlingen, Germany) based on PLS (Partial Least Squares) regression.

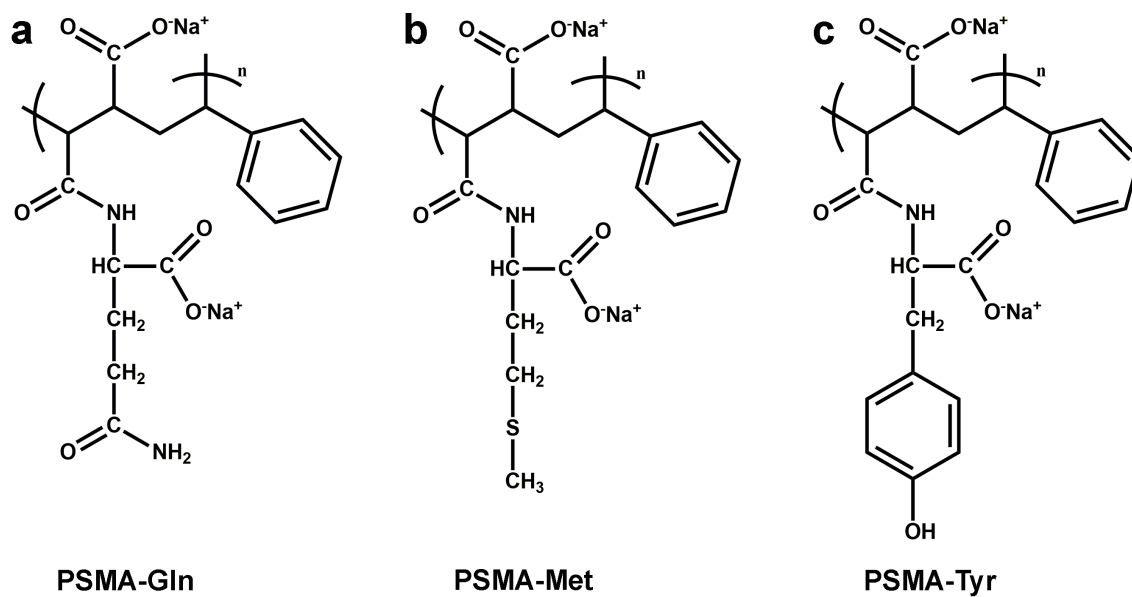
## **2.6 Magnetic Resonance of Proton and Carbon-13 (<sup>1</sup>H-NMR and <sup>13</sup>C-NMR)**

To study <sup>1</sup>H-NMR and <sup>13</sup>C-NMR, ~80 mg of PSMA and of each copolymer functionalized with amino acids were dissolved in DMSO-D6 (0.5 mL). The <sup>1</sup>H-NMR and <sup>13</sup>C-NMR spectra were examined using an Advance-400 spectrometer at 25°C.

## **2.7 Quantitative Elemental Analysis**

Quantitative elemental compositions were determined in an elemental analyzer (CE Instruments, Eager 200 model). The samples were prepared in quantities of 2 mg in tin crucibles, under a constant flow of helium and injection of oxygen gas.

**Scheme 2.** Polyelectrolyte structures: a) PSMA-Gln, b) PSMA-Met, and c) PSMA-Tyr



## 2.8 Polyelectrolyte Adsorption on Solid Surfaces

Polymeric solutions were prepared by dissolving the polyelectrolytes PSMA-Gln, PSMA-Met and PSMA-Tyr in 0.001 M and 0.1 M solutions of NaCl. The pH was adjusted to pH 4.0 and pH 7.0 by adding HCl or NaOH as appropriate. The concentration of the polyelectrolyte solutions varied between  $1.0 \times 10^{-5}$  g/L and 1.0 g/L.

The silicon wafers used as substrates were chemically modified with 3-aminopropyltrimethoxysilane (APTES) by oxidative washing<sup>25</sup> in order to obtain a homogeneous amino acid-terminated monolayer covalently bound to the silicon wafer.<sup>26</sup> Subsequently, the modified silicon wafers were immersed in 2 mL of the polyelectrolyte solutions for 3 h, and then washed with deionized water and dried with an N<sub>2</sub> flow. The quantity of polyelectrolytes adsorbed on the surface was determined by ellipsometry.

## 2.9 Adsorption Isotherms

The adsorption isotherms were obtained by ex-situ ellipsometry in a variable angle ellipsometer L116S300 STOKES (Gaertner Scientific Corporation, USA) equipped with a He-Ne laser with a wavelength of  $\lambda = 632.8$  nm and an angle of incidence,  $\Phi$  of  $70^\circ$  at a temperature of  $25 \pm 1$  °C. The quantity of polyelectrolyte adsorbed  $\Gamma$  was determined according to the relationship between the thickness of the adsorbed layers ( $d_{poly}$ ), the concentration ( $c_{poly}$ ) and the variation of the refractive index of the polyelectrolyte solutions ( $d_n/d_c$ ).<sup>27</sup> The thickness of the adsorbed polyelectrolyte layer was calculated from the ellipsometric angles  $\Delta$  and  $\Psi$  using a multilayer model composed of substrate-medium or substrate-unknown layer (APS or polyelectrolyte film-medium), using the Elli computer program, based on the ellipsometry equation and iterative calculations with Jones matrices.<sup>28</sup> Thus, it is possible to determine only the thickness of the adsorbed polyelectrolyte,  $d_{poly}$ . The small differences in refraction indices  $n$  of the substrate, polyelectrolyte, and solution made an independent determination of  $n_{poly}$  and  $d_{poly}$  impossible. Therefore,  $n_{poly}$  was kept constant as 1.50 and  $d_{poly}$  was calculated.<sup>22</sup> It is important to remember here that, if the index of refraction assumed for the adsorbing polymer layer lies in a reasonable range (between 1.40 and 1.60), the product  $n_{poly} d_{poly}$  should be a constant value.<sup>22, 27</sup> This product is the parameter necessary to calculate the adsorbed amount  $\Gamma$  from equation 1:

$$\Gamma = \frac{d_{poly}(n_{poly}-n_0)}{d_n/d_c} = d_{poly}c_{poly} \quad (1)$$

where  $n_0$  is the refraction index of the solution measured with an Abbe refractometer AR4,  $d_n/d_c$  is the increment of refractive index determined with an interferometric refractometer, and  $c_{poly}$  is the average polyelectrolyte concentration within the layer.<sup>22,27</sup> For the present systems,  $n_0$  was measured for each concentration, and  $d_n/d_c$  amounted to 0.16 mL/g at the temperature of 23

$\pm 1$  °C. The  $dn/dc$  measurements were performed using an OPTILAB DSP interferometric refractometer from Wyatt Technology instruments of sensitivity 0.002 Refractive Index Units.

The refractive indices  $n = 3.88 - i0.018$  for pure silicon,  $n = 1.00$  for air and  $n = 1.462$  for thin layers of  $\text{SiO}_2$  were used to determine the thickness of the  $\text{SiO}_2$  layer. The average thickness obtained after several measurements was  $1.2 \pm 0.2$  nm. To determine the APS monolayer, it is necessary to know the refractive indices  $n = 1.424$  for APS and  $n = 1.00$  for air.<sup>29</sup> The thickness obtained for this layer after several measurements in air was 0.9 - 1.2 nm.

### **2.10 Polymeric Surface Wettability**

The wettability of the polymer surfaces was determined by contact angle measurements on the PSMA, PSMA-Gln, PSMA-Met and PSMA-Tyr films using a Drop Shape Analyzer DSA25S (KRUSS, Germany) using the Sessile Drop method at a temperature of 25 °C. Sessile water drops of 8  $\mu\text{L}$  were used for determine the advancing contact angle ( $\theta_{\text{ADV}}$ ), and then the volume was reduced to 4  $\mu\text{L}$  to measure the receding contact angle ( $\theta_{\text{REC}}$ ). The hysteresis in the contact angle measurements ( $\Delta\theta = \theta_{\text{ADV}} - \theta_{\text{REC}}$ ) was calculated from the difference between ( $\theta_{\text{ADV}}$ ) and ( $\theta_{\text{REC}}$ ). The measurements were performed automatically and controlled by Advance® software (KRUSS, Germany) obtaining images of drop for 1 min, where no changes were observed associated to drop evaporation. At least three spots were done in each sample to make sure we get the same result. Additionally, measurements of contact angle were made using drops of 5  $\mu\text{L}$  in order to rule out effects of volume on the spherical shape and contact angle of the drop.

### **2.11 Polymeric Surface Energy**

Droplets of 5  $\mu\text{L}$  of water, diiodomethane or ethylene glycol were deposited on PSMA-Gln, PSMA-Met and PSMA-Tyr films to determine surface energy. At least three measurements were made for each type of polymer surface with each type of solvent. The surface energy was calculated automatically by Advance® software (KRUSS, Germany) from the water, diiodomethane and ethylene glycol contact angles ( $\theta$ ) obtained once thermodynamic equilibrium was reached (as described by the Young-Laplace equation and the harmonic mean equation proposed by Wu). The latter equation was developed from the surface tension ( $\gamma^{\text{total}}$ ) of a material, considered as the sum of its dispersive ( $\gamma^{\text{D}}$ ) and polar components ( $\gamma^{\text{P}}$ ) that best describe the interactions between a liquid and a polymeric surface with respect to other methods.

30-32

### **2.12 Polyelectrolytes Film Topography and Surface Potential**

The surfaces of the polyelectrolyte films were analyzed by atomic force microscopy (AFM) and Kelvin force microscopy (KFM) with an AFM/SPM Controller 9500 Series System, (Keysight Technologies, CA, USA) with a 7500 scanner. The surfaces were scanned in the magnetic-AC mode (MAC-Mode® Keysight) with a scan rate of 0.3 Hz, using commercial AC200TS three-sided silicon probes (Olympus). The height and amplitude of AFM images were determined at room temperature (23-25 °C). Commercial KS-HQ:XSC11/Pt umasch probes were used for the KFM. All Image analysis and root mean square (RMS) roughness was determined with Keysight PicoView software.

### **2.13 Cells Culture and Cell Viability**

Human SH-SY5Y neuroblastoma cells (CRL-2266, American Type Culture Collection, Rockville, MD) were cultured (humid, 5%  $\text{CO}_2$  atmosphere and 37°C) in MEM-F12 medium

supplemented with 10% FBS, non-essential amino acids, antibiotic–antimycotic mixture, and 20 mM HEPES buffer, at pH 7.2. The cell culture medium was replaced every two days. The effect of the polyelectrolytes on cell viability was quantified by MTT assay following the manufacturer’s instructions. Briefly, 5,000 cells were plated in each well of a 96-well microplate and cultured for 24 hours in the presence of different concentrations of polyelectrolyte solutions (in triplicate). The cell culture medium was replaced with 110  $\mu$ L of fresh medium supplemented with 1,1 mM MTT (3-(4,5-dimethylthiazol-2-yl)-2,5-diphenyltetrazolium bromide) and incubated for 4 hours. Mitochondrial dependent formation of a colored product was terminated by adding 100  $\mu$ L of SDS-HCl solution, followed by 12 hours of solubilization at 37 °C. Absorbance as a measure of product formation was read at 570 nm.<sup>33</sup>

#### **2.14 4-HNE Immunofluorescence**

Oxidative stress induced peroxidation of cell membrane lipids was assayed through immunohistochemistry against 4-HNE.<sup>34</sup> AbCam, UK Poly-clonal antibody ab46545, was diluted 1:200 as indicated by manufacturer's instructions.<sup>35</sup> Briefly, Human SH-SY5Y neuroblastoma cells were seeded on top of clean and sterile acid-washed cover slips<sup>36</sup> or silicon wafers (1x1 cm) coated with fixed substrates (PSMA-Gln, PSMA-MET or PSMA-Tyr) that were UV-sterilized for 15 min. After 24 hours culture, all substrates were washed with phosphate buffered saline (PBS) and fixed for 20 minutes in a 4% paraformaldehyde PBS solution. Cells were permeabilized by a 10 minutes incubation in 0.2% Triton-X-100 PBS solution. Unspecific binding sites were blocked by incubating for 90 minutes in PBS containing 5% (w/v) of bovine serum albumin (BSA, Sigma, USA). Cells were incubated overnight at 4°C with a 1:200 dilution of anti-4 Hydroxynonenal antibody (ab46545; AbCam, UK) in PBS+5%BSA. Substrates were washed three times with PBS (15 minutes), incubated for 90 minutes at room temperature with

Alexa-488-conjugated goat anti-rabbit IgG (1:1000 in PBS-5%BSA), washed three times with PBS (15 minutes) and mounted on glass slides. Glass coverslips were inverted on top of a 25  $\mu$ l drop of mounting medium (FluorSave<sup>TM</sup> (Merk)) while silicon wafers were glued to the glass slide, overlaid with mounting medium and covered with a glass-coverslip. Labeled cells were observed and photographed in a Zeiss LSM 710 confocal laser scanning microscope. Statistical significance was determined using a one-way ANOVA and Tukey post-test.

### **2.15 Scanning Electron Microscopy**

Cells grown on substrates (PSMA-Gln, PSMA-Met or PSMA-Tyr) were fixed with 4% paraformaldehyde, 4% sucrose in saline, permeabilized with 0.2% Triton-X-100 in PBS, incubated overnight at 4°C. Then the samples were then rinsed twice with PBS buffer at pH 7.0 for 15 min and fixed with 1% glutaraldehyde in PBS buffer for 2 h at room temperature. The samples were then rinsed twice in PBS buffer. Finally, the samples were dehydrated in ascending grades of ethanol (30, 50, 70, 80, 90, and 100%) and coated with a thin film of Pt/Pd.

## **3. RESULTS AND DISCUSSION**

### **3.1. Characterization of Polyelectrolytes**

The FT-IR and <sup>13</sup>C-NMR polyelectrolyte spectra were contrasted to the PSMA spectrum to provide a complementary confirmation of the successful modification of PSMA with the different amino acids by opening the maleic anhydride ring and forming an amide bond. The IR spectra (Figures S1-S3 Supplementary Material) show that the characteristic bands of the C=O maleic anhydride PSMA group at 1854  $\text{cm}^{-1}$  and 1779  $\text{cm}^{-1}$  disappear, while two new bands appear at 1664  $\text{cm}^{-1}$  and 1705  $\text{cm}^{-1}$  for PSMA-Gln, 1660  $\text{cm}^{-1}$  and 1703  $\text{cm}^{-1}$  for PSMA-Met, and 1637  $\text{cm}^{-1}$  and 1718  $\text{cm}^{-1}$  for PSMA-Tyr. These represent the stretching of the associated

carbonyl group to an amide, and the stretching of the C=O carboxylic acid group. The  $^{13}\text{C}$ -NMR PSMA spectra (Figures S4-S6 Supplementary Material) show the characteristic signals of the C atoms of the C=O group of the PSMA anhydride at 172.9 and 173.58 ppm. After modification, these signals disappear and signals appear at 174.0 and 178.5 ppm representing the C atoms of the C=O groups of the carboxylic acids and the C=O of the newly formed amide group. The percentages of modification for PSMA-Gln, PSMA-Met and PSMA-Tyr obtained by elemental analysis were respectively 81%, 98% and 80%.

### **3.2. Adsorption of Polyelectrolytes on Amino Acid-terminated Surfaces**

Polyelectrolyte adsorption is strongly influenced by pH level and salt concentration. Adsorption isotherms were obtained at pH 4.0 and 7.0, and at two salt concentrations, 0.1 and 0.001M, to determine the type of interaction that governs adsorption behavior. The polyelectrolyte adsorption rates at pH 4.0 were higher for PSMA-Gln and PSMA-Tyr when the salt concentration was 0.1 M. This behavior is adjusted to what is termed "increased adsorption by shielding", which implies that the forces that modulate the interaction between the surface and polyelectrolyte are mainly of the hydrophobic type and can be explained by the screening of the charged segments of the polyelectrolyte with sodium counter ions. In this case, PSMA-Gln and PSMA-Tyr behave like a neutral polymer, while with PSMA-Met the electrolyte adsorption rate decreases with the salt concentration at 0.1 M. This behavior is determined by the "decreased adsorption by shielding" described by Van der Steeg<sup>37</sup> and implies a modulating force. The interactions between the positively charged amino acid-terminated surface and the -COOH group of the polyelectrolyte are mainly electrostatic.

The polyelectrolyte adsorption rates at pH 7.0 are lower than at pH 4.0, but similar at the two salt concentrations (Table 1, Figure 1) except for PSMA-Tyr. The pK<sub>1</sub> of the PSMA-Tyr carboxylate group is 4.3 lower than the pK<sub>1</sub> of PSMA-Gln and PSMA-Met (see Table 1). The lower pK<sub>1</sub> value of PSMA-Tyr is associated with a larger number of carboxylic groups than with carboxylate groups. Considering that the propyl-amino group on the surface has a pK<sub>a</sub> close to 3.7,<sup>38</sup> it is expected that at pH 7.0 the absence of the amino acid-terminated surface charge promotes H-bonding, and hydrophobic interactions between the phenol of the PSMA-Tyr side chain and the amino acid-terminated surface, increasing the quantity of PSMA-Tyr.

On the other hand, it is well known that the adsorption process is determined by a balance between enthalpy and entropy of the system. In fact, an important theoretical study has shown that the balance between entropic and enthalpic contributions are the forces that drive the adsorption of polyelectrolytes onto surfaces of opposite charge.<sup>39</sup> In this context, the contribution to the enthalpy in the adsorption process implicates in part the water desolvation of the “icelike” around the non-polar moieties of side chain of the polyelectrolyte.<sup>40</sup> This process is endothermic involving small values of enthalpy. However, the adsorption of polyelectrolytes, at the same time is an exothermic process where hydrophobic interactions of the non-polar groups of amino acid residues and of the main chain of polyelectrolytes are promoted with low enthalpy values. Therefore, the total contribution to the enthalpy is low or close to zero and the adsorption process should be determined by the entropy. Rubio et al. analyzed the effect of the molecular architecture of the polyelectrolytes on the adsorption process, finding that the adsorption of the polyelectrolyte is not driven exclusively by the electrostatic interactions, entropic contributions being of fundamental importance, and arise mainly from the release of counterions during the adsorption process.<sup>41</sup> On the other hand, the water desolvation of the non-polar polyelectrolyte

residues in the aqueous solution, results in entropy increase. In this way, the adsorption of a more disordered polyelectrolyte to the surface, as compared with their ordered conformation in solution, also contributes in a gain of entropy for the adsorption process.

Regarding this point, the stability of the films also was studied. The desorption experiments in deionized water at 72 hours showed a reversible adsorption. At pH 4.0, the amount of polyelectrolyte desorbed varied between 15-20% for both ionic strengths, while at pH 7.0 the percent desorption was on average close to 50%. We also determined the adsorption constants ( $K_{ads}$ ) which are summarized in Table S1 (Supplementary Materials), these values are in a range between  $3.15 \times 10^6$  L/mol and  $5.04 \times 10^7$  L/mol which reflect a high affinity of PSMA-Gln, PSMA-Met and PSMA-Tyr with the amino-terminal surface. At pH 4.0, when increasing the ionic strength, an increase of one order of magnitude of  $K_{ads}$  is observed for PSMA-Met and PSMA-Tyr while PSMA-Gln remains constant. At pH 7.0, when increasing the ionic strength, an opposite behavior is observed, where the  $K_{ads}$  values remain practically constant for PSMA-Met and PSMA-Tyr and increase in one order of magnitude for PSMA-Gln. This behavior could be related to the entropic contribution due to the release of sodium counterions during the adsorption process rather than the electrostatic interactions, and also due to the cooperative effect between the first polyelectrolyte chains adsorbed on the following polyelectrolyte chains”.

**Table 1.** Experimental pKapp values for polyelectrolytes and reported pKa values for amino acids

Amino acid	Polyelectrolyte pKapp		Amino acids pKa		Hydropathy index
	pK <sub>app1</sub> -COO <sup>-</sup> group	pK <sub>app2</sub> -COO <sup>-</sup> group	pKa <sub>1</sub> -COO <sup>-</sup> group	pKa <sub>2</sub> -NH <sub>3</sub> <sup>+</sup> group	
Gln	4.90	8.20	2.17	9.13	-3.5
Met	4.90	7.90	2.28	9.21	1.9
Tyr	4.30	8.20	2.20	9.11	-1.3

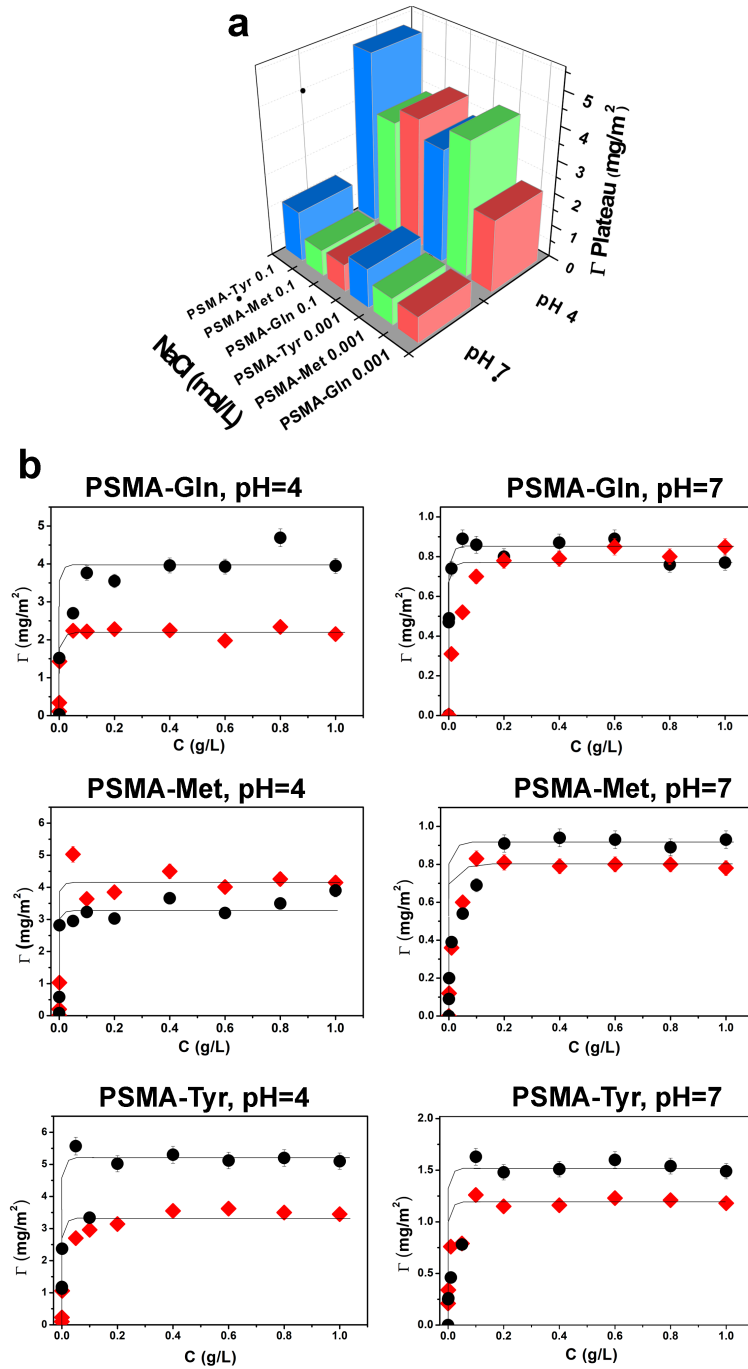


**Figure 1.** (a) Mean quantities of adsorbed polyelectrolytes in the plateau region ( $\Gamma_{\text{plateau}}$ ) at different levels of pH and ionic strengths. (b) Adsorption isotherms obtained for PSMA-Gln, PSMA-Met and PSMA-Tyr on amino acid-terminated surface at pH 4.0 and 7.0 under ionic strength of 0.1 M (black circle) and 0.001 M NaCl (red rhombus).

### 3.3. Polyelectrolyte Films Wettability

**Table 2.** Advancing ( $\theta_{ADV}$ ) and receding ( $\theta_{REC}$ ) contact angles and hysteresis ( $\Delta\theta$ ) in the contact angle for PSMA-Gln, PSMA-Met and PSMA-Tyr of  $6.3 \times 10^4$  g/mol at the 0.5 g/L adsorbed on hydrophilic surfaces at 0.1 and 0.001 mol/L NaCl and at pH 4.0 and pH 7.0

pH	$C_{NaCl}$ (mol/L)	Polyelectrolyte Film	$\theta_{ADV}$ (°)	$\theta_{REC}$ (°)	$\Delta\theta$ (°)
4.0	0.001	PSMA	49±1	59±1	10±1
		PSMA-Gln	67±1	45±1	22±1
		PSMA-Met	60±3	38±2	22±3
		PSMA-Tyr	66±1	47±2	19±2
	0.1	PSMA	51±1	44±2	7±2
		PSMA-Gln	66±1	54±2	12±2
		PSMA-Met	67±2	59±1	8±1
		PSMA-Tyr	69±1	45±1	24±1
7.0	0.001	PSMA	53±2	38±5	15±4
		PSMA-Gln	68±2	41±2	27±2
		PSMA-Met	61±2	40±2	21±2
		PSMA-Tyr	58±1	35±2	23±2
	0.1	PSMA	50±2	31±3	19±3
		PSMA-Gln	72±1	53±1	19±1
		PSMA-Met	74±3	48±1	26±2
		PSMA-Tyr	73±1	50±3	23±2

The advance contact angles ( $\theta_{ADV}$ ) of the polyelectrolyte surfaces using deionized water as a solvent (Table 2) showed moderate effects of ionic strength and pH on the wettability of the polyelectrolytes films. At pH 4.0 and lower ionic strength, there were a larger number of charge groups because screening was reduced. Under this condition, the polyelectrolyte was more extended because charges are repulsed. In this case, PSMA-Gln and PSMA-Tyr adopted loop-like shapes that expose the phenyl group of the main polymer chain to the air, resulting in hydrophobic domains in the polyelectrolyte film. while PSMA-Met exposed the  $-\text{COO}^-$  group of main chain, resulting in a surface with a less hydrophobic character. As was expected, the deprotonated carboxyl groups of the side chain of PSMA-Met interacted with the amino groups of the amino acid-terminated surface through electrostatic interactions. PSMA-Gln H-bonding

between the amino groups of the side chain and the amino acid-terminated surfaces favored exposing hydrophobic residues to the air at pH 4.0 and high ionic strength, so that there was more screening of  $\text{-COO}^-$  groups of lateral and main chain of polyelectrolytes and therefore the polyelectrolytes behaved as neutral polymers when the chains are coiled due to the intra or inter molecular interactions. Under these conditions, the PSMA-Tyr film is hydrophobic, likely because aromatic styrene rings and the side chain are exposed to the air, thus decreasing the wettability of the film and giving it a more hydrophobic character. In the case of PSMA-Met, the low value of the hysteresis angle obtained shows a greater chemical homogeneity in this surface with respect to PSMA-Gln and PSMA-Tyr. This result suggests that the property of wettability of PSMA-Met is given mainly by the exposure of a certain functional group rather than a hydrophilic/hydrophobic balance of the main and lateral chain groups.

A slight effect of the hydrophobic amino acid index on polyelectrolyte wettability is observed at pH 7.0 and the higher ionic strength, while at the lower ionic strength, the PSMA-Gln film is more hydrophobic, even when the Gln hydrophobic index is negative (hydrophilic). This pH value corroborates that the amino groups of the PSMA-Gln side chain interact by H-bonding with the amino groups of the modified surface, leaving a greater number of phenyls of main chain groups exposed to the surface.

In most cases, the polyelectrolytes adsorbed onto the amino acid-terminated surface, exposing a mixture of hydrophilic and hydrophobic groups in their structures, which is reflected in the high hysteresis values, and therefore the surfaces are rather heterogeneous chemically, given the presence of polar groups and hydrophobic residues in the polyelectrolyte structures.

Considering that the highest amount of adsorbed polyelectrolyte occurred at pH 4.0, studies of surface energy, topography, surface potential and cell adhesion were performed on films prepared at pH 4.0 at low and high ionic strength.

### 3.4. Surface Energy of Polymeric Films

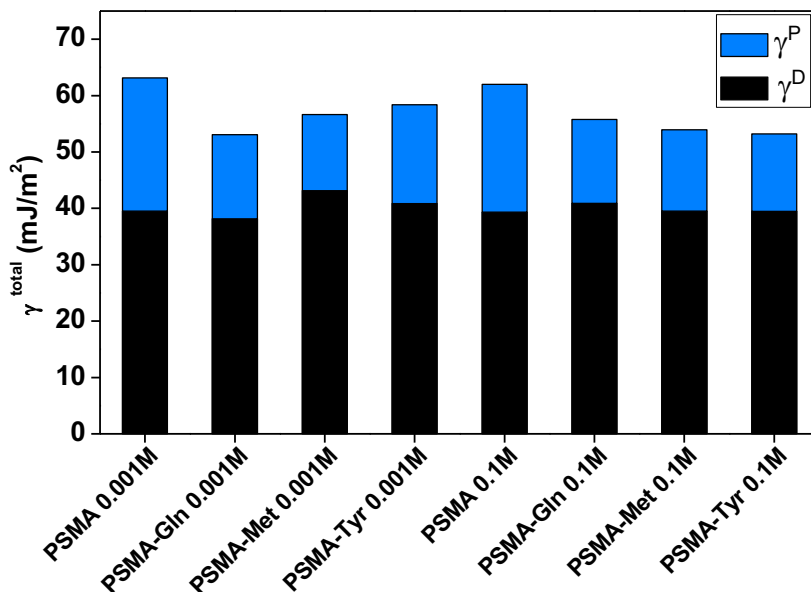
**Table 3.** Advance Contact angles of the water ( $\theta_w$ ), diiodomethane ( $\theta_D$ ) and ethylene glycol ( $\theta_E$ ) and surface energy with polar ( $\gamma^P$ ) and dispersive components ( $\gamma^D$ ) of the polymer films obtained at different ionic strengths at pH 4.0

$C_{NaCl}$ (mol/L)	Polyelectrolyte Film	$\theta_w$ (°)	$\theta_D$ (°)	$\theta_E$ (°)	$\gamma^D$ (mJ/m <sup>2</sup> )	$\gamma^P$ (mJ/m <sup>2</sup> )	$\gamma$ (mJ/m <sup>2</sup> )
0.001	PSMA	49 ± 1	41 ± 1	30 ± 1	41,2 ± 2,91	14,7 ± 6,52	55,9 ± 9,43
	PSMA-Gln	67 ± 1	44 ± 1	47 ± 1	37,6 ± 5,76	6,3 ± 2,55	44,0 ± 8,31
	PSMA-Met	60 ± 3	33 ± 1	37 ± 1	42,5 ± 5,45	8,2 ± 2,93	50,7 ± 8,38
	PSMA-Tyr	66 ± 1	39 ± 1	33 ± 2	39,5 ± 7,25	17,2 ± 3,25	56,7 ± 10,5
0.1	PSMA	51 ± 1	42 ± 1	24 ± 2	40,0 ± 3,69	10,5 ± 1,69	50,4 ± 5,33
	PSMA-Gln	66 ± 1	38 ± 2	40 ± 2	40,9 ± 0,48	7,1 ± 0,89	48,0 ± 1,37
	PSMA-Met	67 ± 2	41 ± 2	38 ± 2	36,6 ± 10,4	11,4 ± 5,08	47,9 ± 15,5
	PSMA-Tyr	69 ± 1	42 ± 3	36 ± 1	39,1 ± 3,81	8,0 ± 1,27	47,0 ± 5,08

Table 3 shows the contact angles obtained using polar-non-polar solvent of water ( $\theta_w$ ), ethylene glycol ( $\theta_E$ ) and diiodomethane ( $\theta_D$ ), and the surface energy determined for the polyelectrolyte films. The surface energy values of all the polyelectrolyte films are relatively similar (in a range of 44 to 56 mJ/m<sup>2</sup>) regardless of the amount of salt added, while the surface energy values of the unmodified polyelectrolyte were slightly higher. The surface energy of organic polymeric materials can be classified as low, medium and high. Low surface energy levels were in the range of 10 to 30 mJ/m<sup>2</sup>. Medium surface energy is between 30-40 mJ/m<sup>2</sup> and solid surface high energy surfaces are above 40 mJ/m<sup>2</sup>.<sup>42</sup> Therefore, the polymer films obtained

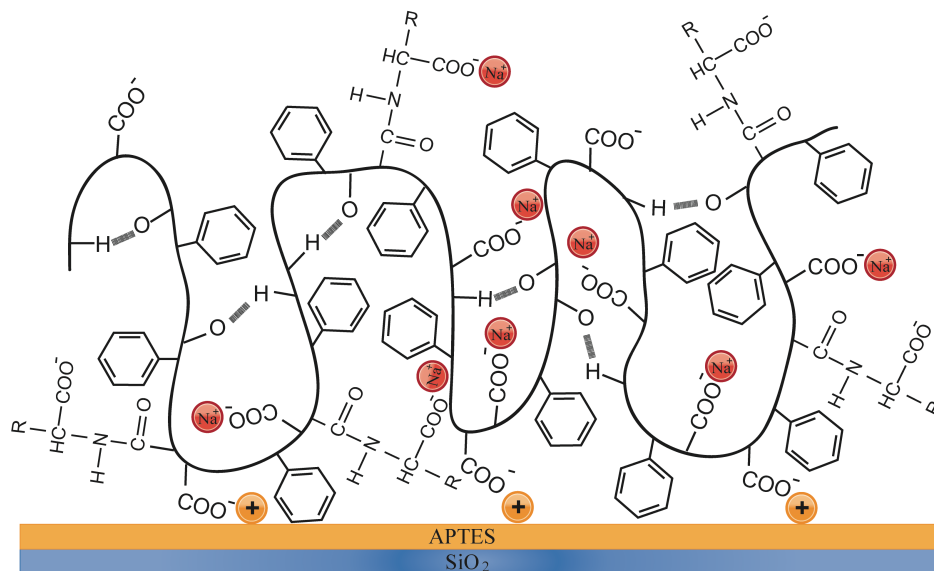
in this work can be considered as having high surface energy. The relative contributions of the components to surface energy ( $\gamma$ ) are determined by the chemical composition of the surface. The polar component ( $\gamma^P$ ) is composed of several polar interactions that include hydrogen bridges, dipole-dipole interaction and induction energy, while the dispersive component ( $\gamma^D$ ) is mainly due to London dispersion forces.

Figure 2 shows that the dispersive component of the surface energy of all the polymeric films is much greater than the polar component, which suggests that the governing interactions are London dispersion forces and to a lesser extent dipole-dipole interactions or hydrogen bridges. This confirms the theory that polyelectrolytes are mainly adsorbed on the surface in a hydrophobic/hydrophilic balance exposing of their side chains and the hydrophobic groups of the main chain to the air, as suggested by the wettability of the films, such as shown Scheme 3.



**Figure 2.** Surface energy ( $\gamma$ ) with the polar ( $\gamma^P$ ) and dispersive components ( $\gamma^D$ ) calculated for PSMA, PSMA-Gln, PSMA-Met and PSMA-Tyr films obtained at different ionic strengths

**Scheme 3.** Graphic representation of polyelectrolytes adsorbed onto amino-terminal surfaces



### 3.5. Polymeric Film Topography, Roughness and Surface Potential

Following the incubation, the grafted APTES silicon surfaces were removed from the polyelectrolyte solution prepared at one of two levels of ionic strength; 0.001 and 0.1 M NaCl, rinsed, and dried with  $\text{N}_2$  stream, and then immediately analyzed by the atomic force microscopy (AFM). The AFM images in Figure 3 show the surface morphology of the polyelectrolyte films on the APTES grafted silicon surfaces after incubation. Very homogeneous and regular polymer deposits are observed in all cases and at both ionic strengths. Two kinds of morphology were adopted, a well-defined globular nanostructure for PSMA-Met and PSMA-Tyr, and a densely packed nanofibrous-like structure for PSMA-Gln. Ionic strength affected the nanostructures forming polyelectrolyte surfaces. Although the surface morphology domains were preserved in both cases, the higher ionic strength value caused a slight decrease in size of the nanostructures forming the surface domains, which was reflected in surface roughness values. Table 4 shows

that for all the electrolytes, surface roughness was greater with the lower ionic strength. At 1mM NaCl, the shielding effect of the  $\text{Na}^+$  counter ion on the charged polyelectrolyte is low and consequently there is a large number of charged groups in polymer network where electrostatic repulsion takes place. These results in the polymer being more extended on the APTES grafted silicon surface, with consequent increased surface roughness. These surface morphology and roughness parameters are consistent with what is described above regarding polyelectrolyte film wettability and surface energy.

Surface potential results using Kelvin force microscopy (frequency modulation) (KFM) for PSMA, PSMA-Gln, PSMA-Met and PSMA-Tyr were respectively 81, 39, 23 and 14mV. These results show higher surface potential values for PSMA and PSMA-Gln. The pKa1 and pKa2 values were respectively 2.9 and 6.4 for PSMA, and 4.3 and 8.2 PSMA-Gln. These values indicate that at pH 4.0 there are groups,  $-\text{COOH}$  and  $-\text{COO}^-$ , with the latter contributing to electrostatic repulsion in the main and lateral chains of the polyelectrolyte. This behavior concurs with the type of 2D nanostructure observed in the PSMA and PSMA-Gln films, which concurs with the low RMS value obtained. It has been reported that an increase in the charge density of a polyelectrolyte induces the adsorption of chains parallel to the surface because a more extended shape is adopted that results in flatter films and a higher surface charge.<sup>43</sup> PSMA-Met and PSMA-Tyr behaved differently where the carboxylic groups (protonated and deprotonated), phenyl groups,  $-\text{S}-$  and  $-\text{CH}_2-$  groups in side chain, generated less repulsion between the charged segments. In this case, hydrophobic interactions and the hydrogen bridge are more important, giving rise to globular nanostructures (3D) that contributed to increased surface roughness. Studies indicate that the correlation between the potential difference and the roughness of

polyelectrolyte films derived from poly(maleic anhydride-*alt*-styrene) depends mainly on the hydrophobic character of the polyelectrolyte side chain.<sup>40</sup>

**Table 4.** RMS of the polymeric films obtained at different ionic strengths at pH 4.0

$C_{\text{NaCl}}$	Polyelectrolyte (mol/L)	Root Mean Square Height (nm)
0.001	PSMA	2.24
	PSMA-Gln	0.59
	PSMA-Met	2.62
	PSMA-Tyr	2.99
0.1	PSMA	1.37
	PSMA-Gln	0.39
	PSMA-Met	2.42
	PSMA-Tyr	2.39

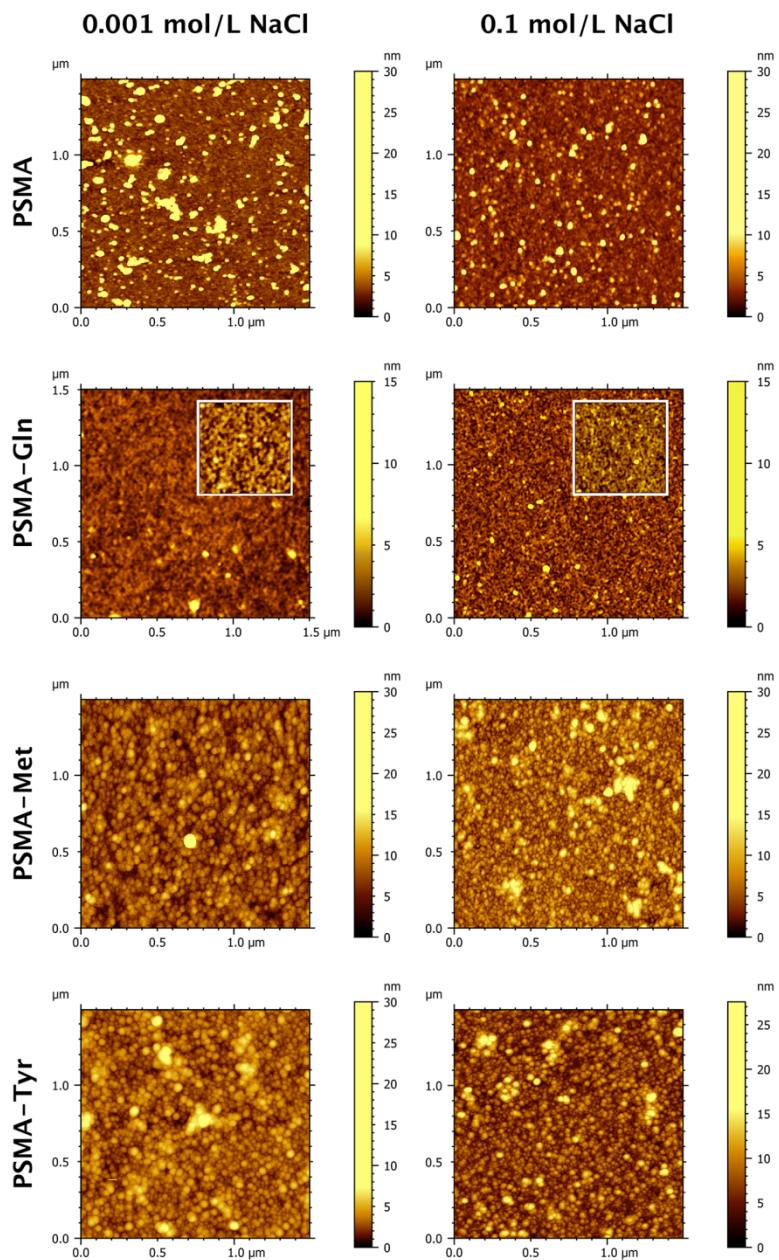


**Figure 3.** AFM images ( $1.5 \mu\text{m} \times 1.5 \mu\text{m}$ ) of the polyelectrolytes adsorbed onto a solid surface at ionic strength of 0.001 and 0.1 mol/L NaCl, at pH 4.0. The inset ( $0.5 \mu\text{m} \times 0.5 \mu\text{m}$ ) on PSMA-Gln images show a zoomed view of polyelectrolytes structure.

### 3.6. Cell Response to PSMA Modified Substrates

25,000 SH-SY5Y neuroblastoma cells were plated on UV-light sterilized PSMA coated silicon surfaces (1 cm<sup>2</sup>), with aforementioned amino acid functionalization. They were compared to cells growing on glass coverslips (in the presence or absence of polylysine). Random fields were photographed under phase contrast microscopy and cells per field was counted in a double-blind fashion at 24, 48 and 72 hours. As can be seen in Figure 4, the cell number per field was consistently and proportionally higher at hour 27 hour/doubling time reported for these cells,<sup>44</sup> suggesting that SH-SY5Y cell proliferation was not significantly affected by the different PSMA modified substrates.

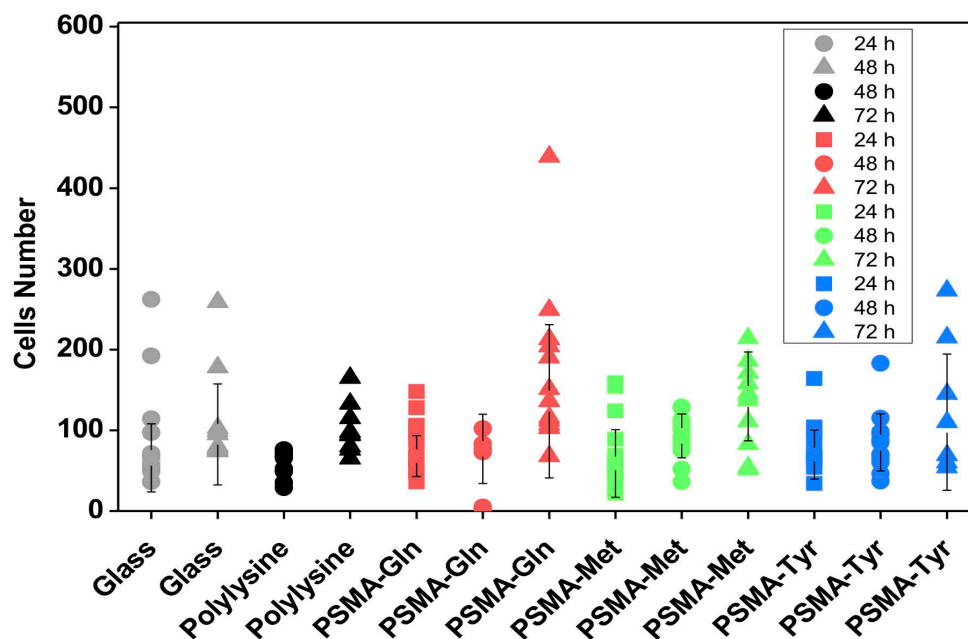


**Figure 4.** SH-SY5Y neuroblastoma cell proliferation is not impaired by different PSMA modified substrates. 25,000 SH-SY5Y neuroblastoma cells were plated and cultured for 24, 48 and 72 hours on different substrates (glass, polylysine-coated glass, PSMA-Gln, PSMA-Met, PSMA-Tyr). Random fields were photographed under phase contrast microscopy and the cell

number was determined in a double-blind fashion. Cell proliferation was not altered in response to the different substrates.

The functionalized PSMA substrates elicited different responses from SH-SY5Y neuroblastoma cells, likely reflecting the differences in hydrophilicity/hydrophobicity of the exposed surface. As can be observed in Figure 5, SH-SY5Y cells spread easily over acid-washed glass coverslips in the absence or presence of a polylysine coating. In contrast, amino-acid functionalized PSMA-polyelectrolytes significantly diminished the spread of cells compared to standard substrates. Only PSMA-Met appeared to induce an increase in lipid peroxidation, which could be interpreted as a stress signal or a change in cell metabolism (Figures 5B and C respectively). Some works have demonstrated the mechanistic aspects of the oxidation by free radicals of sulfur in methionine, which causes lipid peroxidation and formation of reactive oxygen species in neuronal systems.<sup>45</sup> This could suggest that the amino acid residue of methionine in PSMA-Met could have the same effect on neuroblastoma cells. Nevertheless, the treatments did not affect cell viability, as measured by the MTT assay (Figure 5D), which suggests that PSMA-Met modifies SH-SY5Y neuroblastoma response to the substrate.

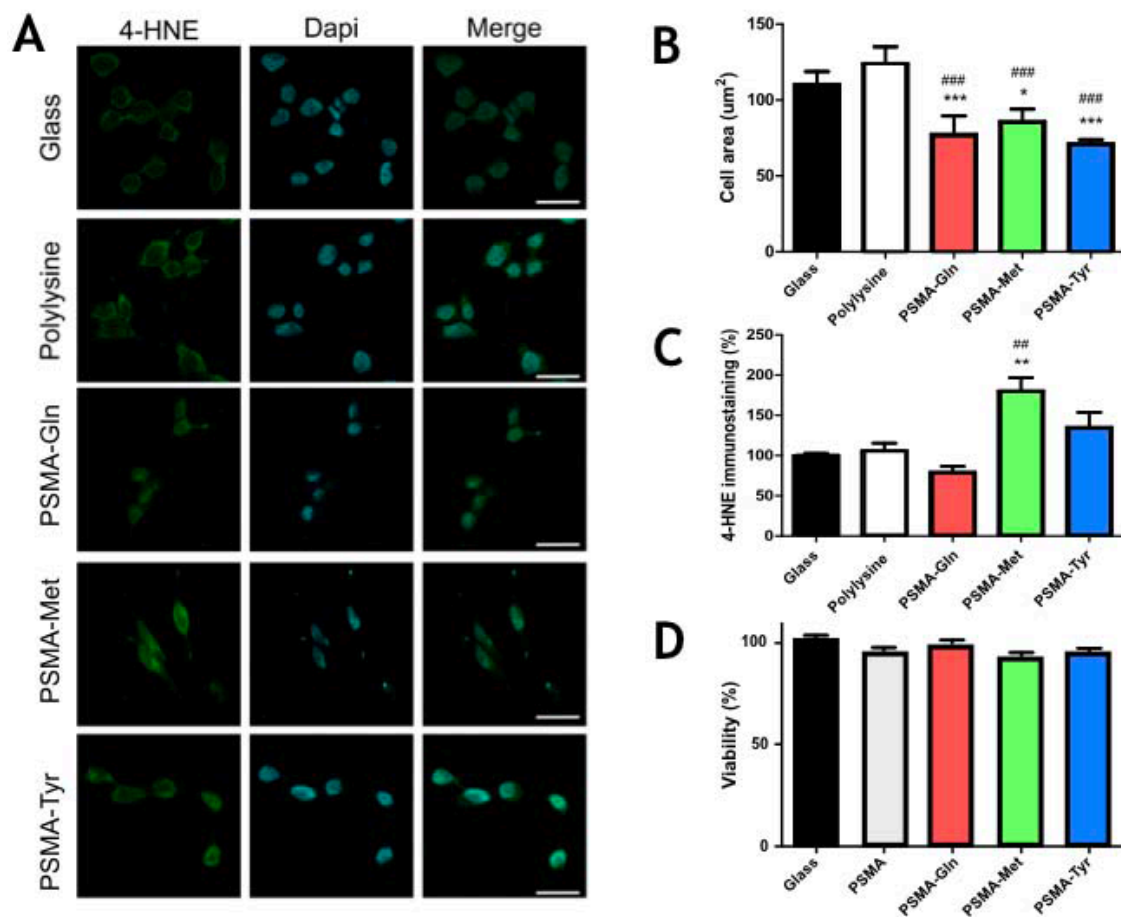


**Figure 5.** The area covered by SH-SY5Y cells on polyelectrolyte-modified substrates were reduced (B), but without altering cell viability. SH-SY5Y cells were plated on different substrates (A) and cultured for 24 hours (37°C, 5% CO<sub>2</sub>). Cells were fixed and stained for immunofluorescence to determine the presence of 4-HNE, a membrane lipid peroxidation marker that indicates damage to cell membranes in response to experimental toxicity (C). Cells identified and counted by DAPI-nuclear staining (405 nm, CYAN) were imaged for 4-HNE and found to be significantly fewer in number than the controls. Only cells plated on PSMA-Met showed a significant increase in lipid peroxidation, which indicates increased oxidative damage. Nevertheless, cell viability, as determined by MTT reduction, was not altered, even when cells were plated on plastic and treated with higher concentrations of polyelectrolytes in solution (D).

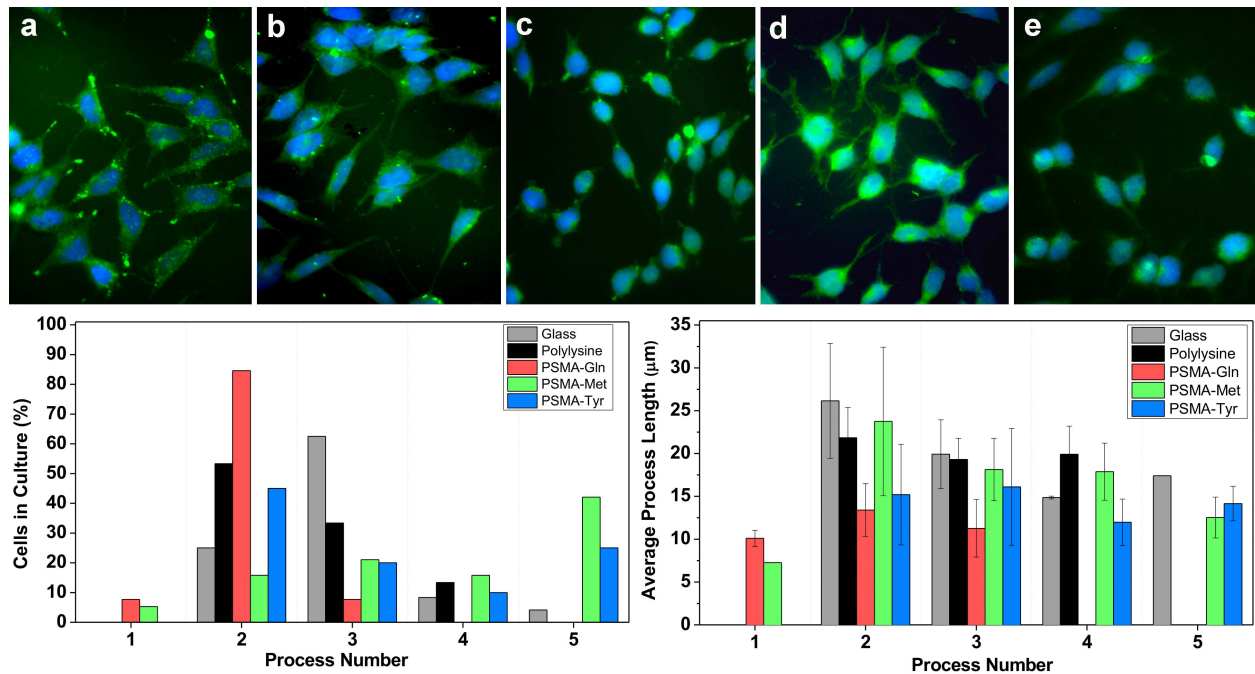


**Figure 6.** SH-SY5Y cultured on (a) glass, (b) polylysine, (c) PSMA-Gln, (d) PSMA-Met and (e) PSMA-Tyr. SH-SY5Y cells responded to PMSA-Met substrates with significant process extension and cell shape remodeling. Control cells a and b, glass and polylysine, respectively had fusiform (two processes) and pyramid (three process) shapes characteristic of undifferentiated neuroblastoma cells. Cells grown on PSMA-Met (d) had a stellate shape, with 5 or more processes, many of which extended over 5  $\mu\text{m}$  from the cell body. Cells grown on PSMA-Gln (c) present fewer and shorter processes.

As can be seen in Figure 6, differences in the shape of SH-SY5Y cells reflects their sensitivity distinct PMSA-substrate characteristics. Control cells (glass and polylysine, respectively) consistently present fusiform (two processes) or pyramidal shapes (three processes) characteristic of undifferentiated SH-SY5Y. These cells also present well defined actin-rich areas that are consistent with focal adhesion. When cultured on PSMA-Met, SH-SY5Y cells present a stellate shape, with 5 or more actin-rich thin processes that extend 5  $\mu\text{m}$  or more from the cell body. In

contrast, when seeded on PSMA-Gln, SH-SY5Y cells have a round morphology, with fewer and shorter processes. The shape suggests that these cells are in a higher state of proliferation, an effect that did not appear to be significant when cell proliferation was assessed (Figure 4). While suggestive, these results do not shed light on whether PSMA-Gln substrates inhibit neuroblastoma cell proliferation or PSMA-Met substrates induce cell differentiation.

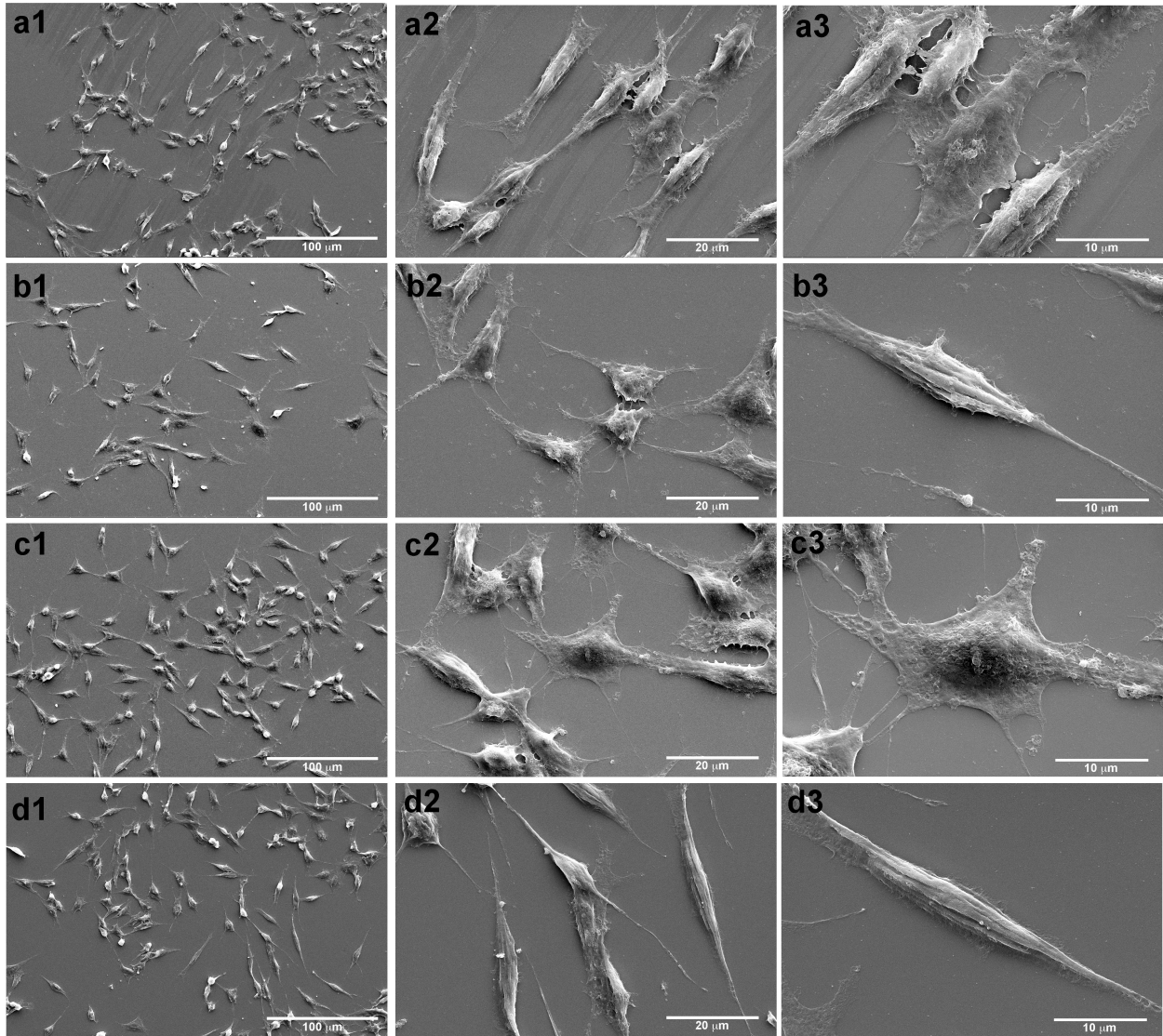


**Figure 7.** SEM images of SH-SY5Y cell cultures after 24 h on (a1, a2, a3) PMSA, (b1, b2, b3) PSMA-Gln, (c1, c2, c3) PMSA-Met and (d1, d2, d3) PMSA-Tyr

Figure 7 shows the morphology of the SH-SY5Y cells cultured on the surface of PMSA, PMSA-Gln, PMSA-Met and PMSA-Tyr. The cells cultured on PSMA-Met have a well-extended morphology, characterized by a much larger cell area than that of cells cultured on PSMA-Gln and PSMA-Tyr, as can be seen in Figure 6. Cells on the surface of unmodified PSMA and PSMA-Tyr have a spindle-like morphology characterized by a small cell area and a high aspect ratio. The well-extended morphology that predominates on the surface of PSMA-Met is associated with its moderate hydrophilicity and topography. Although the hydrophobic index of PSMA-Met is the most positive (hydrophobic), the orientation and conformation of PSMA-Met allows for obtaining a surface of moderate hydrophilicity associated with the heterogeneity of the hydrophilic domains due to its polar (-COOH and -NH<sub>2</sub>) groups in its main and lateral chains. However, the low hysteresis value obtained for PSMA-Met suggests a greater chemical homogeneity of its surface. According to the results of immunofluorescence 4-HNE, a greater response in lipid peroxidation associated with sulfur group present in methionine, would indicate that the chemical nature of the surface of PSMA-Met would be given mainly by the exposure of the groups -S- towards the air, which would participate in the process of oxidation by free radicals. At the same time, PSMA-Met substrates affected cell spreading, increasing the formation of cell extensions in a manner reminiscent of cell differentiation. likely reflecting a cellular response to the low value of hysteresis angle of the exposed surface. Homogeneous overall structure probably provides cells with more attachment sites, thus improving their adhesion to the substrate. While suggestive, these results do not shed light on whether PSMA-Gln substrates inhibit neuroblastoma cell proliferation or PSMA-Met substrates induce cell differentiation. Some works have related the optimal adhesion of neuronal cells with a greater formation of neurites on surfaces of moderate hydrophilicity.<sup>46</sup> The wettability of the surfaces

has been related to the ability of the surface to adsorb proteins from the serum,<sup>47,48</sup> what would facilitate the cell adhesion. Another factor to consider could be related to the roughness of the surface, it has been reported that rougher surfaces achieve a positive response in the cellular adhesion of SH-SY5Y, while other authors have shown that roughness can play minor functions in the response mobile.<sup>49,50</sup> In our case, the roughness of the surface is determined by the effects of repulsion or formation of aggregates given by the presence of charged groups (-COO<sup>-</sup> group) as well as the chemical functionality of polyelectrolytes. The contribution of these effects is reflected in the surface potential values, where the highest values are associated with repulsive effects (PSMA and PSMA-Gln) while the lowest values are related to hydrophobic or hydrogen bridge interactions. For this last case, the associative interactions and roughness would promote the adhesion of SH-SY5Y. In the case of surface energy, the similarity of values between PSMA-Gln, PSMA-Met and PSMA-Tyr would indicate that surface energy is not a determinant physicochemical parameter in the behavior of cell adhesion.

Finally, polyelectrolyte films modified with amino acids of different hydrophobic indices are presented as a simple and low-cost platform, where their properties of wettability, roughness, surface energy and surface potential can be modulated through their chemical functionalization, as well as, the control of the pH and the ionic strength of the medium. The ability to modulate these properties has a direct effect on cell adhesion behavior by observing significant changes in cell processes. The advantage of modulating on simple way the surface properties has not been observed in other polyelectrolyte systems.

## CONCLUSIONS

The adsorption behavior of polyelectrolytes functionalized with amino acids on an amino acid-terminated surface depends on the chemical nature of the polyelectrolyte side chain, its ionic strength and the pH level of the solution. The largest quantity of polyelectrolytes adsorbed was at pH 4.0 and high ionic strength, with more polyelectrolytes adsorbed by the glutamine and tyrosine films than by the methionine film. The contact angle measurements of the polyelectrolyte films showed that wettability at pH 4.0 is governed by the hydrophilic/hydrophobic balance given by hydrophobic domains of the main polyelectrolyte chain, and by the nature of amino acid moiety, while that at pH 7.0 there was an evident contribution of the effect of the hydrophobic amino acid index on polyelectrolyte wettability. The AFM images of polyelectrolyte surfaces showed two kinds of morphology, a well-defined globular nanostructure for PSMA-Met and PSMA-Tyr, and a densely packed nanofibrous-like structure for PSMA-Gln. Cell adhesion assays showed that SH-SY5Y cells cultured on PSMA-Met had a well-extended morphology, characterized by much larger stellate shaped cells, with five or more actin-rich thin processes, while SH-SY5Y cells that were seeded on PSMA-Gln and PSMA-Tyr have a round morphology, with fewer and shorter processes.

These results indicate that it is possible to modulate the surface characteristics of polyelectrolyte films based on their chemical functionality and environmental parameters such as pH and ionic strength, in order to evaluate their effect on cell adhesion.

In conclusion, films obtained from polyelectrolytes functionalized with amino acids can be a simple and low-cost platform for cell adhesion control aimed at developing biomaterials with modified surface properties.

## ASSOCIATED CONTENT

The following files are available free of charge.

Supporting Information: FT-IR spectra of: PSMA and PSMA-Gln, PSMA-Met and PSMA-Tyr.

<sup>13</sup>C-NMR spectra of: PSMA, PSMA-Gln, PSMA-Met and PSMA-Tyr (PDF).

## AUTHOR INFORMATION

### Corresponding Author

† Marcela D. Urzúa, E-mail: maurzua@uchile.cl

† Laura Tamayo, E-mail: laura.tamayo@uchile.cl

### Present Addresses

†Departamento de Química, Facultad de Ciencias, Universidad de Chile, Las Palmeras 3425, Casilla 653, Santiago 7800003, Chile.

### Author Contributions

The manuscript was written through contributions of all authors. All authors have given approval to the final version of the manuscript. These authors contributed equally. M.S. Leal,† X. Briones,† V. Villalobos,◇ Y. Queneau,‡ A. Leiva,§ H.E. Ríos,† J. Pavez,| C.P. Silva,| C. Carrasco,|| Andrónico Neira-Carrillo,∞ A. Roth,|| L. Tamayo,\*† M.D. Urzúa\*†

### Funding Sources

FONDECYT 1151221 and 1100240, FONDECYT Iniciación grant 11160230, ANILLO ACT-1412, PAI-CONICYT 79170015, FONDEQUIP EQM160036.

## ACKNOWLEDGMENT

The authors are grateful to FONDECYT 1151221, FONDECYT 1100240, ANILLO ACT-1412 Project and FONDECYT Iniciación grant 11160230, PAI-CONICYT 79170015, and FONDEQUIP EQM160036.

## REFERENCES

- (1) Waugh, D. G.; Toccaceli, C.; Gillett, A. R.; Ng, C. H.; Hodgson, S. D.; Lawrence, J. Surface Treatments to Modulate Bioadhesion: A Critical Review. *Rev. Adhes. Adhes.* **2016**, *4*, 69-103. <https://doi.org/10.7569/RAA.2016.097304>
- (2) Guo, S.; Zhu, X.; Li, M.; Shi, L.; Ong, J.L.T.; Jańczewski, D.; Neoh, K.G. Parallel Control over Surface Charge and Wettability Using Polyelectrolyte Architecture: Effect on Protein Adsorption and Cell Adhesion. *ACS Appl. Mater. Interfaces.* **2016**, *8*, 30552-30563. <https://doi.org/10.1021/acsami.6b09481>
- (3) Khan, S.; Newaz, G. A Comprehensive Review of Surface Modification for Neural Cell Adhesion and Patterning. *J. Biomed. Mater. Res. A.* **2010**, *93*, 1209-1224. <https://doi.org/10.1002/jbm.a.32698>
- (4) Lee, I. Molecular Self-Assembly: Smart Design of Surface and Interface Via Secondary Molecular Interactions. *Langmuir.* **2013**, *29*, 2476-2489. <https://doi.org/10.1021/la304123b>
- (5) Hardy, A.; Seguin, C.; Brion, A.; Lavalle, P.; Schaaf, P.; Fournel, S.; Bourel-Bonnet, L.; Frisch, B.; De Giorgi, M.  $\beta$ -Cyclodextrin-Functionalized Chitosan/Alginate Compact Polyelectrolyte Complexes (CoPECs) as Functional Biomaterials with Anti-Inflammatory Properties. *ACS Appl. Mater. Interfaces.* **2018**, *10*, 29347-29356. <https://doi.org/10.1021/acsami.8b09733>

- (6) Sanandiya, N. D.; Lee, S.; Rho, S.; Lee, H.; Kim, I. S.; Hwang, D. S. Tunichrome-inspired Pyrogallol Functionalized Chitosan for Tissue Adhesion and Hemostasis. *Carbohydr. Polym.* **2019**, *208*, 77-85. <https://doi.org/10.1016/j.carbpol.2018.12.017>
- (7) Hwang, M. P.; Ding, X.; Gao, J.; Acharya, A. P.; Little, S. R.; Wang, Y. A Biocompatible Betaine-Functionalized Polycation for Coacervation. *Soft Matter*. **2018**, *14*, 387-395. <https://doi.org/10.1039/C7SM01763D>
- (8) Gao, Y.; Xu, Z.; Chen, S.; Gu, W.; Chen, L.; Li, Y. Arginine-Chitosan/DNA Self-Assemble Nanoparticles for Gene Delivery: In Vitro Characteristics and Transfection Efficiency. *Int. J. Pharm.* **2018**, *359*, 241-246. <https://doi.org/10.1016/j.ijpharm.2008.03.037>
- (9) Lv, H. X.; Zhang, Z. H.; Wang, X. P.; Cheng, Q. Q.; Wang, W.; Huang, X. H.; Zou, J. P.; Zhang, Q.; Hou, L. L.; Huo, W. A Biomimetic Chitosan Derivates: Preparation, Characterization and Transdermal Enhancement Studies Of N-Arginine Chitosan. *Molecules*. **2011**, *16*, 6778-6790. <https://doi.org/10.3390/molecules16086778>
- (10) Park, H.; Choi, B.; Nguyen, J.; Fan, J.; Shafi, S.; Klokkevold, P.; Lee, M. Anionic Carbohydrate-Containing Chitosan Scaffolds for Bone Regeneration. *Carbohydr. Polym.* **2013**, *97*, 587-596. <https://doi.org/10.1016/j.carbpol.2013.05.023>
- (11) Ho, M. H.; Wang, D. M.; Hsieh, H. J.; Liu, H. C.; Hsien, T. Y.; Lai, J. Y.; Hou, L. T. Preparation and Characterization of RGD-immobilized Chitosan Scaffolds. *Biomaterials*. **2005**, *26*, 3197-3206. <https://doi.org/10.1016/j.biomaterials.2004.08.032>
- (12) Kim, S.; Cui, Z. K.; Fan, J.; Fartash, A.; Aghaloo, T. L.; Lee, M. Photocrosslinkable Chitosan Hydrogels Functionalized with the RGD Peptide and Phosphoserine to Enhance Osteogenesis. *J. Mater. Chem. B*. **2016**, *4*, 5289-5298. <https://doi.org/10.1039/C6TB01154C>

(13) Tu, H. P.; Lee, X. Q.; Lin, C. Y.; Shen, E. C.; Chen, Y. T.; Fu, E.; Chin, Y. T. Enhanced Attachment and Growth of Periodontal Cells on Glycine-Arginine-Glycine-Aspartic Modified Chitosan Membranes. *J. Med. Sci.* **2016**, *36*, 137. <https://doi.org/10.4103/1011-4564.188898>

(14) LogithKumar, R.; KeshavNarayan, A.; Dhivya, S.; Chawla, A.; Saravanan, S.; Selvamurugan, N. A Review of Chitosan and Its Derivatives in Bone Tissue Engineering. *Carbohydr. Polym.* **2016**, *151*, 172-188. <https://doi.org/10.1016/j.carbpol.2016.05.049>

(15) Jones, D. S.; Laverty, T. P.; Morris, C.; Andrews, G. P. Statistical Modelling of the Rheological and Mucoadhesive Properties of Aqueous Poly (Methylvinylether-Co-Maleic Acid) Networks: Redefining Biomedical Applications and the Relationship Between Viscoelasticity and Mucoadhesion. *Colloids Surf. B.* **2016**, *144*, 125-134. <https://doi.org/10.1016/j.colsurfb.2016.03.008>

(16) Pompe, T.; Zschoche, S.; Herold, N.; Salchert, K.; Gouzy, M. F.; Sperling, C.; Werner, C. Maleic Anhydride Copolymers a Versatile Platform for Molecular Biosurface Engineering. *Biomacromolecules.* **2003**, *4*, 1072-1079. <https://doi.org/10.1021/bm034071c>

(17) Kyte, J.; Doolittle, R. F. A Simple Method for Displaying the Hydrophobic Character of a Protein. *J. Mol. Biol.* **1982**, *157*, 105-132. [https://doi.org/10.1016/0022-2836\(82\)90515-0](https://doi.org/10.1016/0022-2836(82)90515-0)

(18) Kovalevich J, Langford D. Considerations for the use of SH-SY5Y neuroblastoma cells in neurobiology. *Methods Mol Biol.* 2013;1078:9-21. doi: 10.1007/978-1-62703-640-5\_2.

(19) Simpson, P. B.; Bacha, J. I.; Palfreyman, E. L.; Woollacott, A. J.; McKernan, R. M.; Kerby, J. Retinoic Acid-evoked Differentiation of Neuroblastoma Cells Predominates Over Growth Factor Stimulation: An Automated Image Capture and Quantitation Approach to Neuritogenesis. *Anal. Biochem.* **2001**, *298*, 163-169. <https://doi.org/10.1006/abio.2001.5346>

- (20) Morelli, S.; Piscioneri, A.; Messina, A.; Salerno, S.; Al-Fageeh, M. B.; Drioli, E.; Bartolo, L. D. (2015). Neuronal Growth and Differentiation on Biodegradable Membranes. *J. Tissue Eng. Regen. Med.* **2015**, 9, 106-117. <https://doi.org/10.1002/term.1618>
- (21) BC Trivedi, BM Culbertson. Maleic anhydride, Plenum Press, New York (1982)
- (22) Briones, X.G.; Encinas, M.V.; Petri, D.F.S.; Pavez, J.E.; Tapia, R.A.; Yazdani-Pedram M.; Urzúa, M.D. Adsorption Behavior of Hydrophobically Modified Polyelectrolytes onto Amino- or Methyl-Terminated Surfaces. *Langmuir*. **2011**, 27, 13524-13532. <https://doi.org/10.1021/la2025632>
- (23) Ohno, N.; Nitta, K.; Makino, S.; Sugai, S. Conformational Transition of the Copolymer of Maleic Acid and Styrene in Aqueous Solution. *J. Polym. Sci. B.* **1973**, 11, 413-425. <https://doi.org/10.1002/pol.1973.180110302>
- (24) Pretsch, E.; Buehlmann, P.; Affolter, C.; Pretsch, E.; Buehlmann, P.; Affolter, C. **2000**. *Structure Determination of Organic Compounds* (p. 108). Berlin: Springer-Verlag.
- (25) Siqueira Petri, D. F.; Wenz, G., Schunk, P.; Schimmel, T. An Improved Method for the Assembly of Amino-Terminated Monolayers on SiO<sub>2</sub> and the Vapor Deposition of Gold Layers. *Langmuir*. **1999**, 15, 4520-4523. <https://doi.org/10.1021/la981379u>
- (26) Motschmann, H.; Stamm, M.; Toprakcioglu, C. Adsorption Kinetics of Block Copolymers from a Good Solvent: A Two-Stage Process. *Macromolecules*. **1991**, 24, 3681-3688. <https://doi.org/10.1021/ma00012a032>
- (27) De Feijter, J.; Benjamins, D. J.; Veer, F. A. Ellipsometry as a Tool to Study the Adsorption Behavior of Synthetic and Biopolymers at the Air–Water Interface. *Biopolymers*. **1978**, 17, 1759-1772. <https://doi.org/10.1002/bip.1978.360170711>

- (28) Azzam, R. M. A.; Bashara, N. M. Ellipsometry and Polarized Light, North-Holland Publ. Co., Amsterdam **1977**. <https://doi.org/10.1063/1.2994821>
- (29) Urzúa, M.D.; Briones, X.G.; Carrasco, L.P.; Encinas M.V.; Petri, D.F.S. Adsorption of Anionic Amphiphilic Polyelectrolytes onto Amino-Terminated Solid Surfaces. *Polymer*. **2010**, *51*, 3445-3452. <https://doi.org/10.1016/j.polymer.2010.05.054>
- (30) Wu, S. (1971). Calculation of Interfacial Tension in Polymer Systems. In *Journal of Polymer Science Part C: Polymer Symposia* (Vol. 34, No. 1, pp. 19-30). New York: Wiley Subscription Services, Inc., A Wiley Company. <https://doi.org/10.1002/polc.5070340105>
- (31) Wu S. (1982) Polymer Interface and Adhesion: Taylor & Francis; 630 pp.
- (32) Kosaka, P. M.; Kawano, Y.; Petri, D. F. S. Dewetting and Surface Properties of Ultrathin Films of Cellulose Esters. *J. Colloid and Interface Sci.* **2007**, *316*, 671-677. <https://doi.org/10.1016/j.jcis.2007.07.058>
- (33) Mosmann, T. Rapid Colorimetric Assay for Cellular Growth and Survival: Application to Proliferation and Cytotoxicity Assays. *J. Immunol. Methods*. **1983**, *65*, 55-63. [https://doi.org/10.1016/0022-1759\(83\)90303-4](https://doi.org/10.1016/0022-1759(83)90303-4)
- (34) Khan, F.; Moinuddin, Mir A.R.; Islam S.; Alam K.; Ali A. Immunochemical Studies on HNE-Modified HSA: Anti-HNE-HSA Antibodies as a Probe for HNE Damaged Albumin in SLE. *Int J Biol Macromol*. 2016 May;86:145-54. <https://doi.org/10.1016/j.ijbiomac.2016.01.053>. Epub 2016 Jan 19. PubMed PMID: 26800898.
- (35) Abcam.com. (2019). Immunocytochemistry and immunofluorescence protocol | Abcam. [online] Available at: <https://www.abcam.com/protocols/immunocytochemistry-immunofluorescence-protocol> [Accessed 18 Mar. 2019].

(36) Preparation of Slides and Coverslips for Microscopy. Andrew H. Fischer, Kenneth A. Jacobson, Jack Rose and Rolf Zeller Cold Spring Harb Protoc 2008. <https://doi.org/10.1101/pdb.prot4988>

(37) Van de Steeg, H.G.M.; Cohen Stuart M.A.; De Keizer A.; Bijsterbosch, B.H. Polyelectrolyte Adsorption: A Subtle Balance of Forces. *Langmuir*. **1992**, 8, 2538-2546. <https://doi.org/10.1021/la00046a030>

(38) Fujimoto, J.; Petri, D.F.S. Adsorption Behavior of Carboxymethylcellulose on Amino-Terminated Surfaces. *Langmuir*, **2001**, 17,56-60. <https://doi.org/10.1021/la000731c>

(39) Fu, J., Schlenoff, J. B. Driving Forces for Oppositely Charged Polyion Association in aqueous Solutions: Enthalpic, Entropic, but not Electrostatic. *J. Am. Chem. Soc.* 2016, 138, 980-990. <https://doi.org/10.1021/jacs.5b11878>

(40) Briones, X. G.; Urzúa, M. D.; Ríos, H. E.; Espinoza-Beltrán, F. J.; Dabirian, R.; Yazdani-Pedram, M. Thin Films of Amphiphilic Polyelectrolytes. Soft Materials Characterized by Kelvin Probe Force Microscopy. *Polymer*. 2013, 54, 5733-5740. <https://doi.org/10.1016/j.polymer.2013.07.066>

(41) Guzmán, E., Ortega, F., Baghdadli, N., Luengo, G. S., Rubio, R. G. Effect of the molecular structure on the adsorption of conditioning polyelectrolytes on solid substrates. *Colloid Surf. A*. **2011**, 375, 209-218. <https://doi.org/10.1016/j.colsurfa.2010.12.012>

(42) Wake, W. C. (1988). Adhesion and Adhesives: Science and Technology. AJ Kinloch, Chapman and Hall, London.

(43) Llamas, S.; Guzman, E.; Ortega, F.; Baghdadli, N.; Cazeneuve, C.; Rubio, R. G.; Luengo, G. S. Adsorption of Polyelectrolytes and Polyelectrolytes-Surfactant Mixtures at Surfaces: A

Physico-Chemical Approach to a Cosmetic Challenge. *Adv. Colloid Interface Sci.* **2015**, *222*, 461-487. <https://doi.org/10.1016/j.cis.2014.05.007>

(44) Kovalevich, J.; Langford, D. (2013). Considerations for the Use of SH-SY5Y Neuroblastoma Cells in Neurobiology. In *Neuronal Cell Culture* (pp. 9-21). Humana Press, Totowa, NJ. [https://doi.org/10.1007/978-1-62703-640-5\\_2](https://doi.org/10.1007/978-1-62703-640-5_2)

(45) Butterfield, D. A., Kanski, J. Methionine Residue 35 is Critical for the Oxidative Stress and Neurotoxic Properties of Alzheimer's Amyloid B-Peptide 1–42. *Peptides.* **2002**, *23*, 1299-1309. [https://doi.org/10.1016/S0196-9781\(02\)00066-9](https://doi.org/10.1016/S0196-9781(02)00066-9)

(46) Lee, S. J.; Khang, G.; Lee, Y. M.; Lee, H. B. The Effect of Surface Wettability on Induction and Growth of Neurites from the PC-12 Cell on a Polymer Surface. *J. Colloid Interface Sci.* **2003**, *259*, 228– 235. [https://doi.org/10.1016/S0021-9797\(02\)00163-7](https://doi.org/10.1016/S0021-9797(02)00163-7)

(47) Wei, J.; Igarashi, T.; Okumori, N.; Igarashi, T.; Maetani, T.; Liu, B.; Yoshinari, M. Influence of Surface Wettability on Competitive Protein Adsorption and Initial Attachment of Osteoblasts. *Biomed. Mater.* **2009**, *4*, 45002. <https://doi.org/10.1088/1748-6041/4/4/045002>

(48) Arima, Y.; Iwata, H. Effect of Wettability and Surface Functional Groups on Protein Adsorption and Cell Adhesion Using Well-Defined Mixed Self-Assembled Monolayers. *Biomaterials.* **2007**, *28*, 3074– 3082. <https://doi.org/10.1016/j.biomaterials.2007.03.013>

(49) Prévôt, M. E.; Bergquist, L. E.; Sharma, A.; Mori, T.; Gao, Y.; Bera, T.; Zhu, C.; Leslie, M. T.; Cukelj, R.; Korley, L. T. J.; Freeman, E. J.; McDonough J. A.; Clements, R. J.; Hegmann, E. (2017, August). New Developments in 3D Liquid Crystal Elastomers Scaffolds for Tissue Engineering: From Physical Template to Responsive Substrate. In *Liquid Crystals XXI* (Vol. 10361, p. 103610T). *International Society for Optics and Photonics.* <https://doi.org/10.1117/12.2275338>

(50) Genchi, G. G., Ceseracciu, L., Marino, A., Labardi, M., Marras, S., Pignatelli, F., Bruschini, L.; Matolli, V.; Ciofani, G. (2016). P(VDF-TrFE)/BaTiO<sub>3</sub> Nanoparticle Composite Films Mediate Piezoelectric Stimulation and Promote Differentiation of SH-SY5Y Neuroblastoma Cells. *Adv. Healthc. Mater.* **2016**, 5, 1808-1820. <https://doi.org/10.1002/adhm.201600245>

TOC

